Large-eddy simulation of flash flood propagation and sediment transport in a dry-bed desert stream

Abstract

Large-eddy simulation (LES) model is used to study flow dynamics of a flash flood event in a dry-bed desert wash, the so-called Tex Wash, near the Tex Wash Bridge on Interstate 10 in the Mojave Desert of California. The evolving free surface of the flash flood is tracked via the level-set method. A bed morphodynamics module is coupled to the hyrdodynamics model to calculate the erosion and bed evolution of the mobile bed of the wash under the flash flood conditions. Flash floods in a desert wash can be characterized with a number of salient features such as (1) existence of both the dry- and wet-cells on the bed surface of the wash that correspond to the air and water phases, respectively; (2) presence of various flow regimes, critical, sub-critical and super-critical in the flow domain; and (3) occurrence of highly transient and complicated flow field and, subsequently, sediment dynamics throughout the wash. We present a numerical modeling effort to study a recorded flash flood and corresponding scour processes in the Tex Wash. The flood event occurred in 2015 and lead to the collapse of the Tex Wash Bridge. Our goal is to gain insights into the flood flow and sediment transport mechanisms, which resulted in the collapse of the bridge. To that end, we selected a study area which includes a 0.65 km-long reach of Tex wash at its intersection with the Tex-Wash Bridge. The bathymetry of the wash

was obtained via light-detection-and-ranging (LiDAR) technology and used to construct the computational domain of the wash and bridge foundations. The transient flow of the flash flood, in both air and water phases, and the evolving morphology of the wash is numerically simulated. Our site-specific numerical simulation revealed the formation of deep scour regions adjacent to the right abutment of the upstream bridge, where significant erosion caused the collapse of the bridge. Moreover, our results show that most of the scour processes takes place during the steady phase of the flash flood when the wash is filled with water. However, the transient phase of the flash flood is rather short and contributes to a very limited amount of erosion within the wash.
Keywords: Flash flood; dry-bed streams; Large eddy simulations; Sediment transport.

1. Introduction

Excessive rainfalls in a short period of time often cause flash floods in fluvial desert streams. Flash floods are known to be followed by intricate and interconnected hydro- and morpho-dynamics processes. Understanding of these processes seems to be crucial in predicting the effects of flash floods on infrastructures installed within the fluvial desert streams. Flash floods are being considered among the most disastrous natural hazards [6]. As a result, they have attracted significant attention among the researchers in both hydraulic and hydrology fields [34, 11, 29, 46]. Previous studies are primarily focused on understanding the propagation of flash flood to enable development of early warning systems. Such systems seem to enable minimization of hazardous effects of flash floods [7, 38, 32, 12]. This study is focused on flash floods in dry-bed desert streams which can lead to excessive bed erosion around the foundations of infrastructures installed in the stream. Owing to the rarity of water flow in desert streams, bridge and other infrastructure foundations are often placed in shallow depth of stream bed which renders these structures vulnerable to even small amounts of scour during flash floods.

Past studies of flash flood propagation are mainly focused on hydrological modeling approaches. For instance, Knocke [27] proposed a localized lumped hydrological model embedded into geographic information systems (GIS) enabling effective flood forecast and risk assessment. Julien et al. [14] introduced a physically-based distributed model, TREX, and demonstrated its ability to simulate watershed processes by applying to three filed studies. In order to improve predictive capabilities of flash flood models for arid regions, Al-Rawas and co-workers [1, 2] conducted GIS-based studies of flash flood in Oman. Schaffner et al. [41] applied the real-time distributed KINematic runoff and EROsion model (KINEROS2) to predict the rainfall and basin response of the Fish Creek basin in California, to evaluate the ability of this model. By comparing the result to sub-daily measured data and result of MARINE model, Boithias et al. [5] tested the ability of the sub-daily module of the lumped Soil and Water Assessment Tool (SWAT) to simulated discharges in a catchment. Hydrological models are very easy to be solved by computer so that they are efficient to predict flood event.

Hydrodynamic models are potentially capable of predicting more complex phenomena, such as transient flow and sediment dynamics. To study the physical mechanisms of flash flood and predict water depth and velocity field more accurately, past studied have, for the most part, focused on hydrodynamic models. For instance, Mudd [36] performed a scaling analysis and developed a numerical model coupled one-dimensional (1D) Saint-Venant equations and Richards' equation, to investigate flow and infiltration in ephemeral channels during flash flood. Cao et al. [9] developed a 1D shallow water hydrodynamic model to reveal the self-amplifying mechanism of the interaction between the flow and bed scour and the active sediment transport by flash flood. Abderrezzak et al. [10] used a two-dimensional (2D) depth-averaged shallow water model to study flash flood propagation in urban areas. Despite some discrepancies observed around buildings where the flow is strongly three-dimensional (3D), their results show good accordance with experimental data. Using a 2D shallow water hydrodynamic model, Roca and Davison [40] analyzed blockage of structures and changes in flow dynamics during a flash flood. Kvocka et el.[30] studied three different 2D hydrodynamic models; i.e., models based on: simplified version of the 2D shallow water equations, full 2D shallow water equations, and full hydrodynamic 2D models with shock-capturing ability; and determined a general threshold value of the bottom slope as an guideline for selecting adequate flood model. Xia et al. [45] discussed the challenges encountered by overland flow simulations, and developed a numerical scheme based on the full 2D shallow water equations to simulate large-scale transient overland flood flows. Hu and Song [13] developed a 2D shallow water model for simulation of flash floods in mountain watersheds, and executed it in

GPU-based parallel model. Liu et al. [33] applied a coupled 1D and 2D hydrodynamic model linking the channel flow and watershed for flood simulation over a complex terrain. They employed 1D Saint-Venant equations were for the channel flow, while 2D shallow water equations were adopted to simulate floods in the basin. Bricker et al. [8] investigated flood prediction strategies in a data-scare environment, and compared 1D HEC-RAS model and 2D Delft-FLOW model. They showed that the 1D model generates conservative results while running faster, whereas 2D model is more accurate and, thus, useful for hazard assessment. Li et al. [31] developed a 3D dydrodynamic model based on Reynolds-averaged Navier-Stocks equations including hydrodynamic pressure to simulate flood flows and assess the flood risk. Albano et al. [3] applied a 3D free-mesh Smoothed Particle Hydrodynamics (SPH) model to investigate rigid body movement in flash flood. Using the Stevens Institute of Technology Estuarine and Coastal Ocean Model (sECOM), Marsooli et al. [35] studied coastal flood mitigation by vegetation which is a 3D model based on Reynolds-Averaged NavierStokes (RANS) equations with hydrostatic pressure distribution. Such hydrodynamic simulations often require relatively high computational resources, especially for extensive geographical domains. Thus, researchers have attempted to develop hybrid methods which combine the hydrodynamic modeling and hydrological approaches. For example, Kourgialas and Karatzas [28] developed an integrated modeling system for the estimation of flood flow velocity and sediment transport. This system combined hydrological model HSPF (Hydrological Simulation ProgramFORTRAN), the quasi-2D distributed MIKE 11 hydrodynamic module and the MIKE 11 suspended sediment transport module. The impact of riparian vegetation on flash flood propagation was then studied using this modeling system. Nguyen et al. [37] developed a high resolution coupled hydrologic-hydraulic model for flash flood modeling, the so-called HiResFlood-UCI. Also, Bellos and Tsakiris [4] developed a hybrid model by combining the hydrological unit, hydrograph theory, and a physically-based 2D hydrodynamic model, the so-called FLOW-R2D.

Although flash floods are extensively studied, few of past studies are focused on 3D interactions of flash flood, sediment transport, and terrain and infrastructures. Taking advantage of recent advances in computing technology and parallel processing on computing clusters, we attempted to numerically model a flash flood event in a desert wash, the Tex wash in the Mojave Desert of California. The flash flood of interest occurred on July 15, 2015 causing significant damage to the Tex Wash Bridge located on Interstate 10 in California. As seen in Fig. 1 and reported in [43], the bridge failure is occurred because of the severe bed scour around the bridge foundations leading to human fatality and great economic loss. The objective of this study is to better understand the dynamics of the flash flood encroachment on the dry-bed of the wash and its effect on the sediment transport and scour processes throughout the wash and, particularly, around the collapsed hydraulic structures. When the head of a flash flood enters the dry-bed flow domain, it propagates downstream until the wash is filled up with flood water. The period before the wash is filled is denoted as transient phase. Soon after transient phase is over, the steady phase of the flash flood starts. We note that the duration of the transient phase is solely a function of flash flood's mean-flow velocity and geometric characteristics of the wash. However, the duration of the steady phase is a function of the flood hydrograph. In this work, a constant volumetric flow rate at the inlet cross-section of the domain is considered. The chosen flow rate is equal to that of the peak of the flood flow. Such an inlet boundary condition was as a result of that the hydrograph of flash flood event is not known. We expect that such an inlet flow rate will lead to conservative results for the scour depth around the hydraulic structures located in the wash. The mean-flow velocity at the inlet is considered to be equal to 0.5 m/s. Our simulation results show that the head of the flash flood propagates with a variable speed of 1 to 3 m/s. Given the fact that the length of the study area in the wash is about 0.65 km, the flash flood has a transient phase of $\approx 5\ min$. The total duration of the flood was recorded to be about 10 hours and the duration of steady phase of the flash flood is 9 hours and 55 minutes. The duration of the transient phase is less than one percent of that of steady phase of the flash flood. The effect of flash flood during both the transient and steady phases on the sediment transport around the bridge foundations was the subject of the study.

This paper is organized as follows. The governing equations are introduced in Sec. 2. Subsequently, the computational details of the simulation are presented in Sect. 3. Then, the computed results for the instantaneous flow field of the flash flood are presented in Sec. 4. In the same section, the bed morphodynamics simulation results are also presented and discussed. Finally, the main contribution of the paper is summarized in Sec. 5.

2. Governing equations

2.1. Flow solver

Turbulent flood flow is solved using the spatially-filtered continuity and Navier-Stokes equations in both the air and water phases using LES model. The governing equations in non-orthogonal, generalized, curvilinear coordinates $\{\xi^i\}$ read as follows:

$$J\frac{\partial U^j}{\partial \xi^j} = 0 \tag{1}$$

$$\begin{aligned}\frac{1}{J}\frac{\partial U^j}{\partial t} = & \frac{\xi_l^i}{J}\left[-\frac{\partial\left(U^j u_l\right)}{\partial \xi_j} + \frac{1}{\rho(\phi)Re}\frac{\partial}{\partial \xi^j}\left(\mu(\phi)\frac{\xi_l^j \xi_l^k}{J}\frac{\partial u_l}{\partial \xi^k}\right) - \frac{1}{\rho(\phi)}\frac{\partial}{\partial \xi^j}\left(\frac{\xi_l^j p}{J}\right)\right. \\ & \left. -\frac{1}{\rho(\phi)}\frac{\partial \tau_{lj}}{\partial \xi^j} - \frac{\kappa}{\rho(\phi)We^2}\frac{\partial h(\phi)}{\partial x_j} + \frac{\delta_{ij}}{Fr^2}\right]\end{aligned} \tag{2}$$

where the transformed equations are in compact tensor notation in which the repeated indices imply summation. ξ_l^i are the transformation metrics, J is the Jacobian of the transformation, U^i is the contravariant volume flux, u_i is the Cartesian velocity component, p is the pressure, τ_{lj} is the sub-grid scale (SGS) tensor, κ is the curvature of the interface, and δ_{ij} is the Kronecker delta. ρ, μ, ϕ and h are the fluid density, the viscosity, the level set function, and the smoothed Heaviside function, respectively. Re, Fr, and We are the dimensionless Reynolds, Froude, and Weber numbers, respectively:

$$Re = \frac{UL\rho_{water}}{\mu_{water}}, Fr = \frac{U}{\sqrt{gL}}, We = U\sqrt{\frac{\rho_{water}L}{\sigma}} \tag{3}$$

where U and L are the characteristic velocity and length of the flash-flood flow, g is the gravitational acceleration, and σ the surface tension. ρ_{water} and μ_{water} are the density and dynamics viscosity of the water phase, respectively.

The water/air interface of the flash-flood flow is tracked by solving for the level-set function $\phi(x, y, z, t)$ as a scalar that defines the minimum distance from any computational cell center within the fluid domain to the closest point on the water/air interface, where the iso-surfaces of ϕ is equal to zero. To ensure numerical stability of solution, the fluid properties at the water/air interface are smeared over a thin layer. Details of the level-set method, LES turbulent model, and numerical methods employed in the flow solver are already reported elsewhere and, for the sake of brevity, we refer the reader to [15, 25, 20].

2.2. Sediment transport solver

The temporal variation of the bed elevation is governed by the Exner-Polya equation:

$$(1-\gamma)\frac{\partial z_b}{\partial t} = \underbrace{-\nabla \cdot \mathbf{q}_{BL}}_{Bed-load} \tag{4}$$

where γ is the sediment material porosity, z_b is the bed elevation, ∇ denotes the divergence operator, and $\mathbf{q}_{BL}$ is the bed-load flux vector, which is calculated as follows [21]:

$$\mathbf{q}_{BL} = \Psi \left\| d\mathbf{S} \right\| \delta_{BL} \mathbf{u}_{BL} \tag{5}$$

where Ψ is the local sediment concentration on the mobile bed surface (computed using Van Rijn formala [39]), $\|d\mathbf{S}\|$ is the length of the bed cell edge, δ_{BL} is the thickness of the bed-load layer (considered to be equal to $20d_{50}$, where d_{50} is the median grain size of sediment material [24]), and $\mathbf{u}_{BL}$ is the flow velocity vector parallel to the bed surface at the edge of the bed-load layer. At each time step, once the flow field is computed (on the background structured mesh), velocity field and bed shear stress info are projected onto the cell centroids of bed surface (unrestricted triangular grid) at the edge of bed-load layer using the law of the wall (for more details, see [42]). As flash flood propagates downstream, the Exner-Polya equation is solely solved for bed cells that are covered by water, i.e. wet cells. At each time step, the wet cells are found and flagged using a search algorithm which uses fluid density adjacent to the bed cell to differentiate water from air (see Fig. 3). Furthermore, the model employs a sand-slide algorithm to correct the slope of bed surface whereever it exceeds the angle of repose of the bed material. Details of these algorithms can be found in [26]. Finally, it is important to mention that the coupling between the flow solver and bed morphodynamics calculations is done by adopting a fluid-structure interaction (FSI) approach. Detailed description of this FSI approach is already reported in [21].

3. Computational Details

We employ our in-house coupled flow and bed morphodynamics model, the Virtual Flow Simulator (VFS-Geophysics) code, to simulate the flash flood and, consequently, sediment transport in the Tex wash. The flash flood is modeled in the three phases of air, water, and sediment – in a fully coupled manner. The two former phases are resolved to track the free surface of the flash flood, as its head propagates through the wash. Using the large eddy simulation (LES) model, the flood-induced turbulence is resolved [25]. Free surface of the flash flood is modeled using the level-set method [15, 20]. Once resolved, the hydrodynamics of the water flow over the dry-bed of the wash is used to resolve the latter phase using a bed morphodynamics module that is coupled with the flow solver. A surface bed-cell on the wash bathymetry, under dry-bed condition, can be in contact with either water or air. Sediment transport is allowed to occur on the bed cells that are in contact with water, i.e., wet-bed cells. To that end, a module is developed to identify the wet- and dry-bed cells and, subsequently, sediment transport solely on the wet-bed cells is to be solved. As shown in Fig. 2, the study area within the Tex wash consists of a highly complex bathymetry with several bridge piers of the Tex-Wash bridge. The bridge foundations are located in a ≈ 27 m-wide narrow channel, where the highway intersects with the wash. The complex geometry of the wash and the bridge piers are obtained using light-detection-and-ranging (LiDAR) technology and considered in the simulations using the curvilinear Immersed Boundary (CURVIB) module of the VFS-Geophysics model. The flow field of the flash flood of July 15, 2015 is modeled on a structured background mesh within a 0.65 km-long reach of the wash. The calculation area is shown with the black rectangle in Fig. 2(D). Nevertheless, the sediment transport calculations are carried out on the unstructured triangular grid system. This area is limited to a 0.25 km-long portion of the wash on the both sides of the Tex-Wash Bridge – see the refined triangular mesh region around the bridge piers in Fig. 2(E). As seen in the figure, near the inlet section of the study area, the wash is relatively narrow (≈ 50 m wide). Farther downstream, the wash becomes wider reaching a maximum width of about 200 m. The wider area of the wash includes a relatively deep gorge close to the right bank of the wash, while the dry-bed of the wash near the left bank is rather elevated generating a relatively shallow water condition–see next section. The wide region of the wash ends to the narrow channel. It is noted that the transition from the wide region of the wash to the narrow gorge includes a sharp bend, which is expected to generate a system of energetic helical flow within this region. Additionally, the interaction of such helical flow with the bridge piers in the narrow channel can induce highly complicated flow dynamics. As reported [43], extreme erosion near the right bank of the narrow channel adjacent to the bridge foundation "P2" (see Fig. 2) has led to the failure of the right abutment then the collapse of the bridge span. It seems to be of great importance to employ a finer grid resolution around the bridge foundations to understand the effect of flash flood on the scour pattern near the bridge abutment and the link between the flow dynamics and scour process in this region. Employing proper grid systems, a fully coupled hydro- and morphodynamics numerical simulation is conducted to gain insights about the dynamics of the interaction of the flash flow, the wash bed, the side banks, and the bridge foundations. Such insight would potentially be helpful for a better understanding of the effects of the flash flood on structural stability of our infrastructures.

Fig. 4 plots the Cartesian background mesh, which is used to discretize the flow domain, along with the unstructured triangular grid system for discretization of the immersed bodies: stream morphology and bridge foundations. Table 1 presents the details of these grid systems along with the temporal steps used in the simulations. As seen in this figure, the Cartesian background mesh is uniform in vertical, while stretched horizontally with a stretching factor of 1.05 to better resolve the areas of interest: regions around the bridge foundations.

The selected time-step for the flow solver ($\Delta t \approx 0.005s$) leads to a the maximum Courant-Friedrichs-Lewy (CFL) number of 0.1 ensuring numerical stability of the flow and free-surface computations of the flash flood. Desynchronizing the flow and sediment transport computations (while still fully coupled), a morphodynamics time-step of $\Delta t_s \approx 1000 \times \Delta t$ was selected for the sediment transport model. This dual time-stepping approach allows for affordable and yet physical simulation of the evolution of bed morphology of the stream for longer periods of time. Details of the dual time-stepping algorithm along with its validation studies are reported in [23].

For the inlet boundary condition, we employ a flux of 14 m^3/s at the inlet cross plane of the domain resulting in a mean-flow velocity of $\approx 0.5m/s$ at the inlet. Neumann boundary condition is employed for velocity components and pressure at the outlet cross plane, while the velocity field at the sediment/water and solid/water interface of the wash bathymetry and bridge foundations is reconstructed using a wall modeling approach [26]. The large-scale roughness's on the river banks and on the bed are directly incorporated in the flow field calculations through immersed boundary method, while their surfaces are treated as rough surfaces with an effective roughness height of $20d_{50}$. Sediment transport is recirculated within the computational domain by setting the inflow of sediment at the inlet section equal to that of outflow of the sediment mass at the outlet section.

The coupled three-phase flow simulations in this work are performed on a supercomputing cluster, the so-called "Zagros", at the Department of Civil Engineering of Stony Brook University. Zagros has 76 compute nodes with 1216 cores. Cores are 3.06 GHz Intel X5675 with 6 GB RAM/core and connected via QDR Infiniband. The cluster has a 135 TB Lustre-based storage system with distributed meta data servers (MDS) and object storage servers (OSS), all connected via the IB network in order to handle high I/O needs of the code. For this work, we employed 512 cores for 15 days of CPU-time to simulate 10h of actual time of the flash flood.

4. Results and discussions

4.1. Instantaneous flash-flood flow

Prior to present the computed flow field, it is important to note that the wash bathymetry is highly irregular with complex macro-roughness elements. Based on the concept of specific energy in open-channel flows, variations in the bed geometry can lead to changes in water depth and geometry. Therefore, the interaction of a flash flood with such irregularities in the wash is expected to induce variations in the flow depth and, consequently, velocity field. The simulation results of instantaneous velocity field is presented at the free surface of the flash flood within the study area (Fig. 5). In the middle of the wash, just downstream of the inlet cross-section, the LES has captured a jet-like flow which has a high-velocity core with velocity magnitudes of up to 5 m/s (Fig. 5(A and C)). As it impinges upon the road shoulder, the high-velocity region ends with a hydraulic jump. Immediately downstream of the hydraulic jump, the flash flood enters the sharp, near 90^o, bend and flows towards the bridge foundations, "P1" and "P2". Entering the narrow channel, the flash-flood markedly accelerates. The dynamics of the flood flow within the narrow channel is quite intricate because of its interaction with the side banks, bridge foundations, and the irregularities in the bank geometry–to name a few. The flow in the narrow channel also contains a high-energy 3D helical flow, which is induced by the sharp bend at the entrance to the narrow channel. These features led to a very complex flow field around the bridge piers. For instance, note the local hydraulic jump at point i and ii, as seen in Fig. 5(B). This local hydraulic jump seems to be formed because of the local flow acceleration between the bridge pier "P1" and the right bank of the narrow channel. Overall, the Fr number in the narrow channel is shown to be varying significantly, from 0.1 to 7, inducing simultaneously sub-critical, super-critical and critical flow regimes (Fig. 5(D)). Note the computed flow field near the left bank of the narrow channel, where the flow is relatively less accelerated. As seen in Fig. 5(B and D), at farther downstream regions, in the wake of bridge piers "P3" and "P4", flash flood forms another jet-like flow with a high-velocity core near the mid-wash region.

In Fig. 6, the computed instantaneous flow field is plotted at the mid-depth of the flash-flood flow. As seen in this figure, the velocity magnitudes within the narrow channel is roughly as high as those observed at the free surface. The high velocity region near the right bank of the narrow channel is noted – all the way, from the beginning to the end of the narrow channel (see Fig. 6(B)). We expect such high velocity core to impose high shear forces on the right bank threatening its stability. Another high-velocity core is captured in the middle of the narrow channel, between the two adjacent bridge piers. The velocity magnitude near the left bank of the narrow channel, however, is relatively small. Additionally, computed contours of the out-of-plane vorticity component are illustrated in Fig. 6(C). As seen in this figure, the flow contains a wide range of high-energy vertical structures within the narrow channel. The dominant vortical structures between the right bank and the bridge piers "P2" and "P4" is noted. The two counter-rotating vortexes are the reminiscent of the helical vortex formed because of the sharp bend – see Fig. 6(C).

We plot in Fig. 7 contours of dimensionless bed shear stress, i.e., Shield's parameter ($= \tau_o / [(\rho_s - \rho) g d_{50}]$, where τ_o and ρ_s are the bed shear stress and the sediment density, respectively). For a channel bed to act as a mobile bed, the Shield's parameter should be higher than its critical value, θ_{cr}. Based on the sediment material size of the wash, θ_{cr} is equal to 0.028 [44]. The bank erosion can be attributed to high values of the Shield's parameters near the bank – due to highly energetic turbulent flow and increased mean flow gradients in that region [22]. As seen in Fig. 7(A and B), the computed Shield's parameter near the right bank is quite higher than the critical value of 0.028, whereas the Shield's parameter at the left bank is slightly smaller than or equal to θ_{cr}. It is also noted that, in the region between the bridge piers, θ is significantly higher than the critical value. As seen, the computed bed shear stress distribution within the narrow channel show that, in most locations with the narrow channel, θ is greater than the threshold value, therefore significant bed material movements is to be expected. In the next section, the computed bed morphology will be presented and analyzed to examine the effect of the flash flood on the transport of bed material within the wash.

4.2. Sediment transport calculations

In this section the morphodynamics results of the coupled flow and bed simulations are presented to examine the effect of the flash-flood flow on the evolution of the wash morphology. First, the initial bathymetry of the wash, prior to the flash flood event, is presented (Fig. 8). As seen, the initial bed topography of the wash around the bridge foundation has variable longitudinal slope with an average of $\approx 5\%$, which is relatively steep.

In Fig. 9, the computed bed topography of the wash is plotted at the end of the steady phase of the flash flood, i.e. $t \approx 10\ h$. As seen, the LES model obtained a deep scour depth near the base of the banks and around the bridge piers "P1" and "P2". The LES model captured a number of sand waves, which propagate downstream. These sand waves are formed near the entrance of the narrow channel migrating downstream of the wash. As seen in Fig. 9(A), after $t \approx 10\ h$, they are located downstream of the bridge piers "P3" and "P4". There are a number of salient features vis-*à*-vis the computed results of bed morphology in Fig. 9. These features include: (*i*) sediment transport process at locations upstream of the narrow channel is rather insignificant and, therefore, the bed topography of the wash in these regions has experienced the least amount of bed change; (*ii*) interaction of the sharp-bend-induced-3D-helical flow and the accelerated flash-flood flow leads to a significant bed material moment in the narrow channel, all the way from its beginning to end; (*iii*) as a results, significant amount of scour takes place immediately at the base of the right bank near the bridge pier "P1"; and (*iv*) the wash bed at the base of the left bank, which is less exposed to the helical flow, experiences relatively smaller scour.

In order to further investigate the amount of bed-elevation change through the wash bed, we calculate the bed-change parameter, Δz_b. This parameter, calculated locally for each bed cell, represents the difference between the bed elevation of the wash at the beginning and the end of the sediment transport process. Hence, the bed-change parameter is obtained as $\Delta z_b = z_{end} - z_{init}$ in which z_{init} is measured in the field and used as the initial bed-topographic condition and z_{end} is the computed bed-topography after 10 h of the flash flood. The contours of computed bed-change parameter is shown in Fig. 10. As seen, the bed-change at the region upstream of the narrow channel hovers around zero. Likewise, the bed-change of the narrow channel downstream of the bridge piers "P1" and "P2" experiences either no scour or sediment deposition. While, the base of the right bank, near the bridge pier "P2", is among the zones where maximum scour depths can be observed. To be exact, the maximum computed scour depth is ≈ 1.8 m, which corresponds to the base of the right bank – see Fig. 10(B). It is important to note that the location of the computed maximum scour depth is in accord with the region at which the bridge foundation failure reportedly led to the collapse of the Tex-Wash Bridge during the flash flood, as seen in Fig. 1. Similarly, a deep scour region can be observed upstream of the bridge pier "P1", however, since there was no field field measurements, these predicted scour patterns cannot be validated. Overall, one can argue that the complex flow with elevated turbulence level in the narrow channel has led to deep scour around the bridge foundations – see the intricate water surface, velocity field, and bed shear stress distribution in Figs. 5, 6, and 7, respectively. Given the drop of the water surface around bridge piers "P1" and "P2" (Fig. 5), we argue that the deep scours at this location are caused by the accelerated flow and high shear stress near the inlet of the narrow channel [16, 17, 18, 19].

Now, the evolution of the computed bed-morphology during the 10 h-long flash flood event is examined. To do so, the time history of the computed sediment-transport kinematics is analyzed at a local point on the bed surface, where the information during the flood are recorded. The local point is picked to be between the tip of the bridge pier "P2" and the right bank because of the importance of the scour at the right bank of the narrow channel. This point is denoted as "th" and shown with a pink star in Fig. 8.

The computed time history of the sediment-transport kinematics at the point "th" on the bed surface of the wash is plotted in Fig. 11. In this figure, the first ≈ 5 min of the time histories, during which the bed surface is in contact with air, is skipped. In Fig. 11(A), the time history of the velocity magnitude of the sediment phase is showed at the boundary of the bed-load layer, i.e., sediment/water interface. As seen, starting from a velocity magnitude of ≈ 0.7 m/s, the velocity magnitude gradually reduces to about 0.45 m/s. Fluctuating slightly around these values after about 3 h, the velocity magnitude of particles seems to be at a dynamic equilibrium. A similar trend can be seen for the time history of the Shield's parameter in Fig. 11(B) where the two models reach quasi-equilibrium after about 3 h while the computed Shield's parameter fluctuates around $\theta \approx 0.06$. Both the sediment phase velocity and Shield's parameter are proportional to the flow velocity. Hence, the decreasing trend of the Shield's parameter and sediment phase velocity is due to the reduction in the flow velocity, owing to the deformation of the stream bed and the expansion of the cross-sectional area of the flow. It is noted that the critical value of Shield's particle in this work is $\theta_{cr} \approx 0.03$, which is half of the Shield's parameter at equilibrium and indicates that sediment in this location is rather mobile. The time history of the rate-of-change of the bed elevation, $\partial z_b/\partial t$ is shown in Fig.

11(C). The rate-of-change represents the instantaneous time-variation of the bed elevation. Multiplied by the time-step of the sediment transport model (Δt_s), the rate-of-change of the bed can be quantified in meter (m). As seen in this figure, early on, the rate-of-change is ≈ -8 mm meaning that the bed elevation is scouring by 8 mm at each time step. Rapidly decreasing, the rate-of-change diverges to a minimal amount of ≈ -1 mm each time step. We also plot in Fig. 11(D) the time history of the sediment bed-load (q_b) per unit width of the channel. As seen, a trend very similar to that of the Shield's parameter can be seen for the q_b, which after about 3 h reaches a quasi-equilibrium value of ≈ 0.3 $kg/s/m$. The association between θ and q_b is something to be expected, as it is a general characteristic of all continuum, or Eulerian, sediment transport models. Also, Figs. 11(E and F) depict the time history of the bed elevation and scour depth (H_s). The two parameters are essentially the same because the instantaneous H_s is defined as $H_s = z_b - z_{init}$, in which z_b is the instantaneous bed elevation at the point "th", while z_{init} is a constant value that is equal to the initial value of z_b at point "th". Unlike all other parameters whose time histories converge after ≈ 3 h, the time histories of z_b and H_s include continuously descending and ascending limbs, respectively. In other words, had we continued the simulations beyond 10 h duration of the flash flood, the scour depth would increase further. This means that although the morphodynamics parameters (i.e., V, θ, q_b, and $\partial z_b/\partial t$) have reached quasi-equilibrium after 3 h, nonetheless the bed elevation computations are not at equilibrium yet. This characteristic can be specific solely to flash flood events in desert, dry-bed, wash in which Fr number varies so drastically throughout the waterway. Having said that the slopes of the time history lines of both z_b and H_s seem to be reducing and that they seem to eventually plateau. Finally, the contribution of the transient phase to overall scour depth can be seen in Fig. 11(F). The red dashed line in this figure shows the time when the transient phase of the flash flood is over ($\sim 5\ min$). The local scour depth at this time is about 3.7 cm that is less than two percent of the total scour depth at the end of the flood. This is mainly because the transient phase takes only about 5 minutes, which is less than one percent of the flash flood duration. Thus, one can argue that the overall contribution of the transient phase of the flash flood to the scour and streambed deformation is insignificant.

5. Conclusions

A fully-coupled hydrodynamics and morphodynamics model, the VFS-Geophysics code, is employed to simulate numerically the three-phase flow of air, water, and sediment in a dry-bed desert wash under flash flood conditions. The wash, the so-called Tex wash, is located in the Mojave Desert of California. The simulated flash flood, which is the subject of this study, was caused by an intensive rainfall on July 15, 2015. The simulation domain is limited to a 650 m-long reach of the Tex wash at its intersection with Interstate Highway 10. The flash flood event, after about 10 h flood duration, led to the collapse of the bridge infrastructure, the so-called Tex-Wash Bridge, causing significant economic loss and endangering public safety.

We attempted to use the VFS-Geophysics model to gain insight into the mechanisms that lead to the collapse of the bridge. The site-specific numerical simulation of the Tex wash was carried out by taking into account detailed geometry of the wash bathymetry and bridge foundations. It started by allowing the head of the flash flood to propagate through the wash filling the study area. The free surface of the flash flood was traced using the level-set method. Otherwise, the turbulent flow of the flood was resolved using the LES model. This model, coupled with the morphodynamics module of the VFS-Geophysics code, was helpful to quantify the flash flood kinematics, flow, and sediment dynamics in the wash within the study area. The computed flow field results revealed the formation of highly complicated flow dynamics within the study area with all the flow regimes of critical, sub-critical, and super critical taking place, simultaneously. Moreover, our flow field computations using LES revealed the formation of two major hydraulic jumps. One of these hydraulic jumps occurs at a location between the bridge pier "P2" and the right bank of the narrow channel, which leads to a super-critical and high-velocity core Jet-flow immediately adjacent to the base of the right bank of the narrow channel. The morphodynamics results also revealed the development of a deep scour region adjacent to the right bank of the narrow channel, where the hydraulic jump took place. These finding agree well with the reported accident at the Tex-Wash Bridge, where erosion of the right bank foundation led to the collapse of the bridge. The grid resolution of our LES was selected to be rather coarse to enable the simulation of such real-life stream. However, higher resolution LES can be utilized to gain more insightful information into the interaction of flash floods, stream bed and banks, and the infrastructures.

The site-specific, fully coupled, numerical simulation of the flash flood event in the Tex wash illustrates clearly the capability of LES to provide

Table 1: The computational grid systems and the time step employed for the flow and morphodynamics solvers. N_{x_i} and Δx_i ($\forall i = 1, 2, 3$) (in m) indicate the number of grid nodes and the finest grid spacing of the background grid for flow solver in the i direction, respectively. y, x, and z represent streamwise, spanwise, and vertical directions, respectively. $\Delta z^+ = u_* \Delta z/\nu$ is the minimum grid spacing in the vertical direction scaled in inner wall units. Shear velocity, u_*, is calculated from wall model calculations. Δt and Δt_s (both in s) are the temporal steps of the flow and morphodynamics modules, respectively. N_f is the number grid nodes (background mesh) to discretize the flow domain. While, N_s is the numbers of unstructured triangular cells to discretize the wash bathymetry and bridge foundations. ΔS (in m) is the finest edge size of the unstructured triangular cells used in the bed morphodynamics calculations.

$N_x \times N_y \times N_z$	Δx	Δy	Δz	Δz^+	Δt	ΔS	Δt_s	N_s
$541 \times 1101 \times 61$	0.15	0.18	0.10	$> 10^3$	0.005	0.45	5.0	1.8×10^6

science-based predictions revealing the effects of flash floods on infrastructures. Such predictive tools have the potential to obtain invaluable knowledge to be utilized by engineers and practitioners to protect vulnerable infrastructures against natural hazards, e.g. the flash flood of July 15, 2015 at the Tex wash and, consequently, prevent similar disastrous incidents.

Acknowledgments

This work was supported by NSF award EAR-1823121. The computational resources were provided by the Center for Excellence in Wireless and Information Technology (CEWIT), College of Engineering & Applied Sciences at Stony Brook University.

Figure 1: Pictures of the Tex Wash Bridge taken two days after the collapse of the bridge. Note the excessive erosion at the base of the right bank of the wash. (A) views upstream of the wash and shows the bridge piers herein denoted as "P1" and "P2". (B) is taken immediately upstream of the bridge piers, views downstream of the wash, and is focused on the collapsed right bank adjacent to the bridge pier "P2".

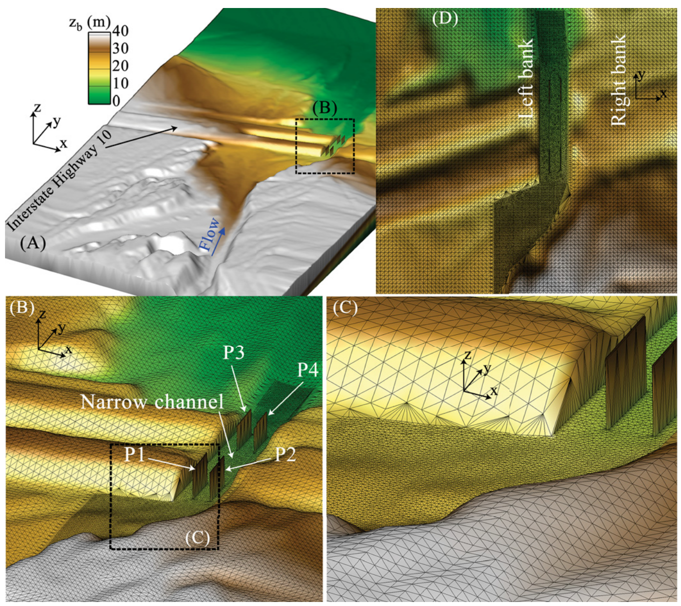

Figure 2: An aerial view of the study area in the Tex wash colored with bed elevation (z_b) showing the bridge piers on Interstate Highway 10. (A), (B), and (C) represent successive zoomed-in views of the study area in 3D. (D) is a zoomed-in view of the study area from top view.

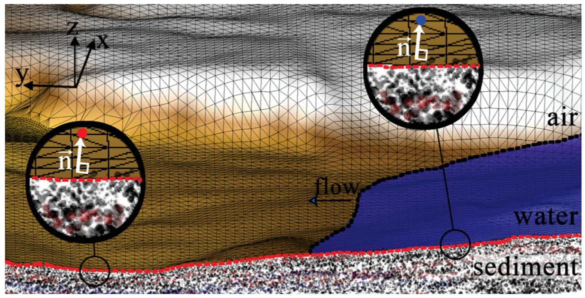

Figure 3: Schematic of the flash flood flow over a dry-bed fluvial stream. The flow field, for both the air and water phases is solved on the background mesh that contains sediment, water, and air phases. Unstructured triangular mesh represents the bathymetry of the wash. Bed morphodynamics equations are solved at the sediment/fluid interface (dashed-red line). Level-set method is used to track the location of the free surface (dashed-black line) of the flash flood. Normal vectors ($\vec{\mathbf{n}}$) are radiated from the bed-cell surfaces into the background mesh to identify the wet- (blue dot) and dry-bed (red dot) cells on the bed surface of the wash.

References

[1] G.A. Al-Rawas, C. Valeo, Issues with Flash Flood Modeling in the Capital region of Sultanate Oman, Geomatics Engineering, Schulich School of Engineering, University of Calgary (2008) 1–11.

[2] G.A.A. Al-rawas, Flash flood modelling in Oman wadis, Ph.D. thesis, University of Calgary, 2009.

[3] R. Albano, A. Sole, D. Mirauda, J. Adamowski, K.E.K. Abderrezzak, A. Paquier, E. Mignot, Modelling large floating bodies in urban area flash-floods via a Smoothed Particle Hydrodynamics model, Journal of Hydrology 541 (2016) 344–358.

[4] V. Bellos, G. Tsakiris, A hybrid method for flood simulation in small

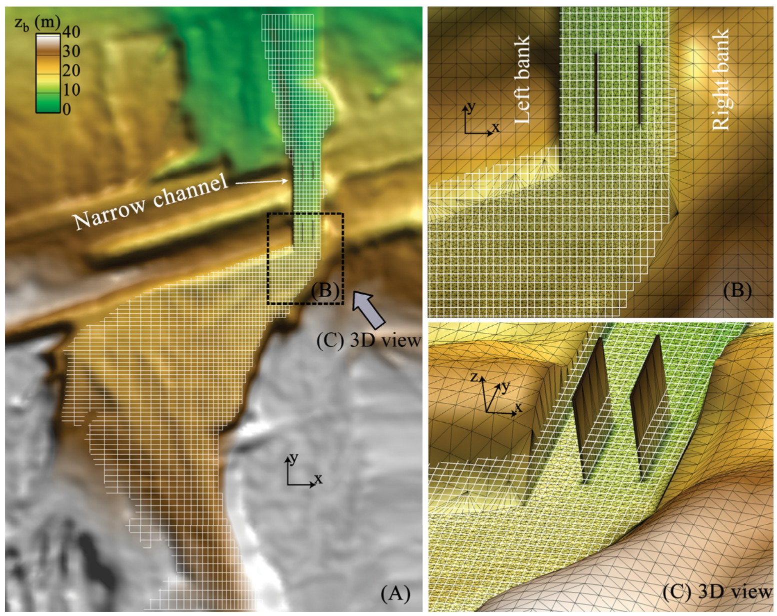

Figure 4: Computational grid systems for discretizing the wash bathymetry, bridge foundations, and flow domain of the study area. The structured mesh (white lines) of the background grid system to discretize the flow domain is shown at the z equal to the maximum elevation in (A), in which only every other 10 computational cells is showed. Zoomed-in views of the grid systems around the bridge piers are shown in a plan and 3D in (B) and (C), respectively. In addition, the unstructured triangular grids (black-lines triangles) for discretization of wash bathymetry and bridge foundation can be seen in (B) and (C). In (B) and (C) we present every other 5 computational cells of the background mesh system.

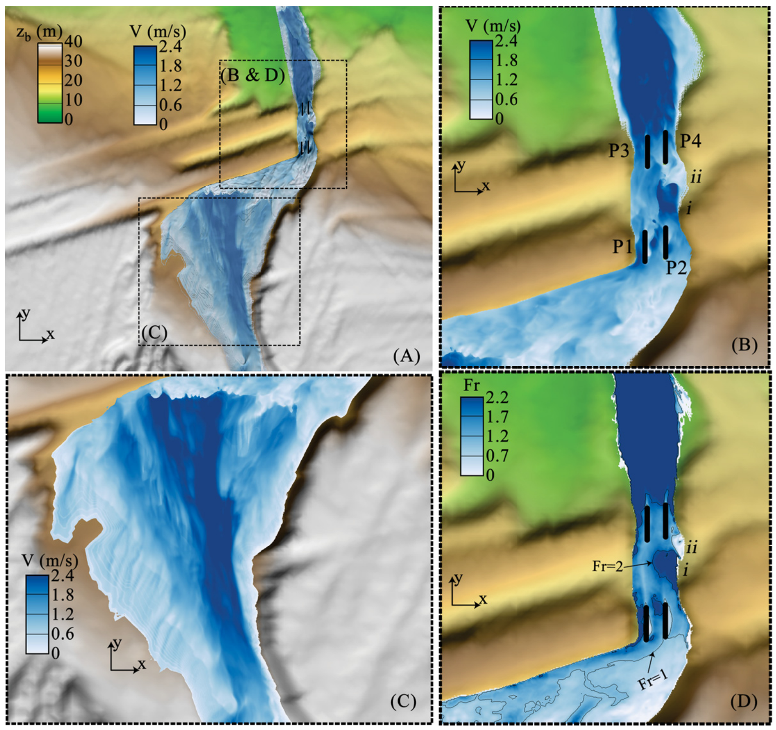

Figure 5: Computed instantaneous flow field of the flash flood in the Tex wash at the water surface. (A) shows the contour of the velocity magnitude (V) and the bed elevation (z_b) of the wash. The zoomed-in view of (B) shows the contour of velocity magnitude around the bridge piers "P1" and "P2" within the narrow channel. In the zoomed-in window of (C), the contours of velocity magnitude is presented. Near the upper part of this window, one can see the hydraulic jump. The zoomed-in window of (D) shows the Fr number distribution in the wash. The flash flood flows from bottom to top.

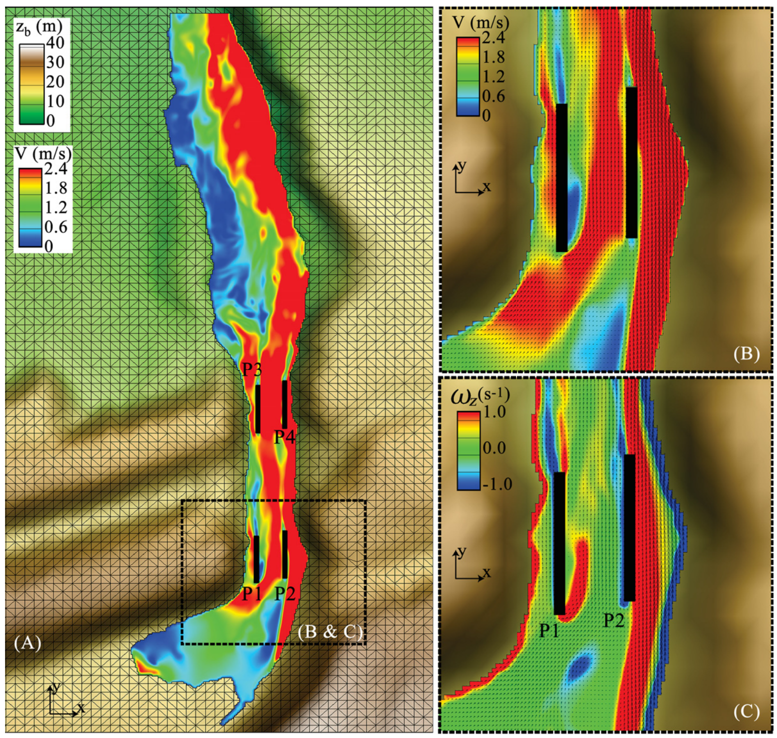

Figure 6: Computed instantaneous flow field at the mid-depth of the flash flood in the Tex wash from top view. (A) shows the contour of the velocity magnitude (V) and the bed elevation (z_b) of the wash. The zoomed-in view of (B) shows the contour of velocity magnitude, along with the velocity vectors, around the bridge piers "P1" and "P2" within the narrow channel. The zoomed-in window of (C) presents the contours of out-of-plane vorticity component (ω_z). The flash flood flows from bottom to top.

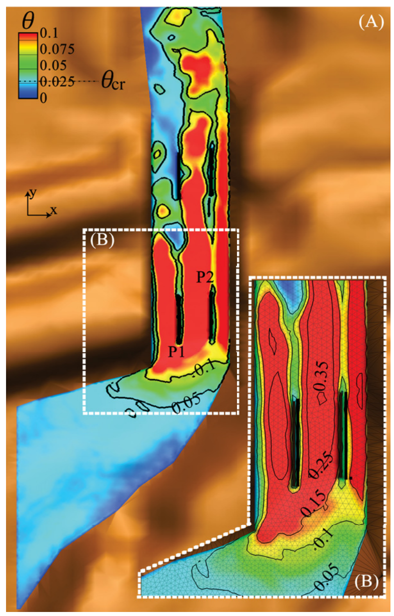

Figure 7: Computed contours of instantaneous, dimensionless, bed shear stress (i.e., Shield's parameter, θ) in the Tex wash from top view. The zoomed-in view of (B) shows the distribution of θ around the bridge piers within the narrow channel. The critical value of the dimensionless bed-shear-stress for sediment movement is equal to $\theta_{cr} = 0.028$. The triangular grids in (B) and (D) are the grid systems used to discretize the morphodynamics equations. The flash flood flows from bottom to top.

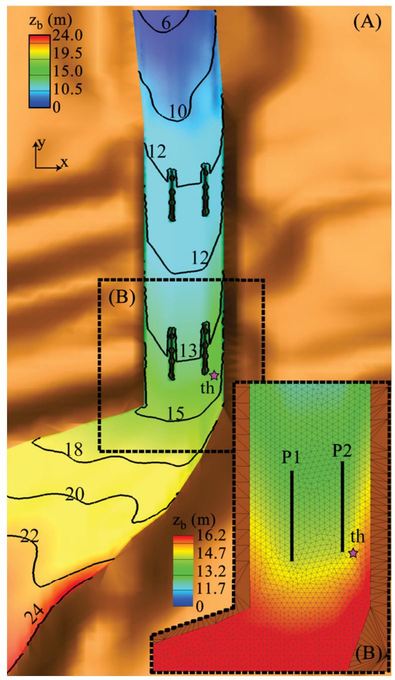

Figure 8: Bed bathymetry and contours of bed elevation (z_b) of the Tex wash within the study area (A) where the bed morphodynamics equations are solved. (B) shows details of the bed topography around the bridge piers "P1" and "P2". The pink-star in (A) and (B), denoted as "th", represent the location on the wash bed where the time history of the sediment phase kinematics are recorded. Contour-line labels are in m. The flash flood flows from bottom to top.

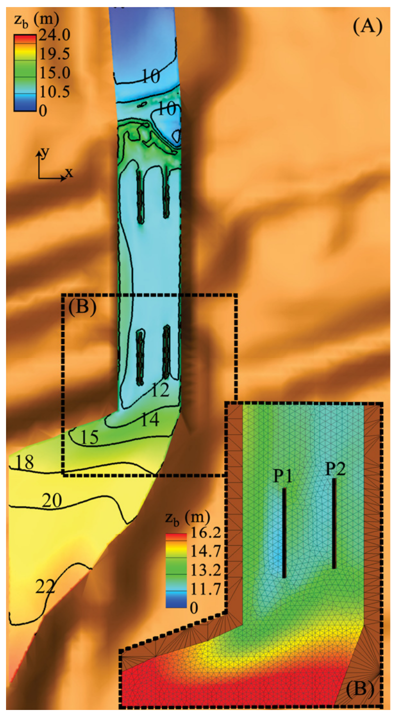

Figure 9: Computed bed topography and contours of bed elevation (z_b) of the Tex wash within the study area after $t = 10$ h of the flash flood (A). (B) shows a zoomed-in windows illustrating details of the computed bed topography around the bridge piers "P1" and "P2". Contour-line labels are in m. The flash flood flows from bottom to top.

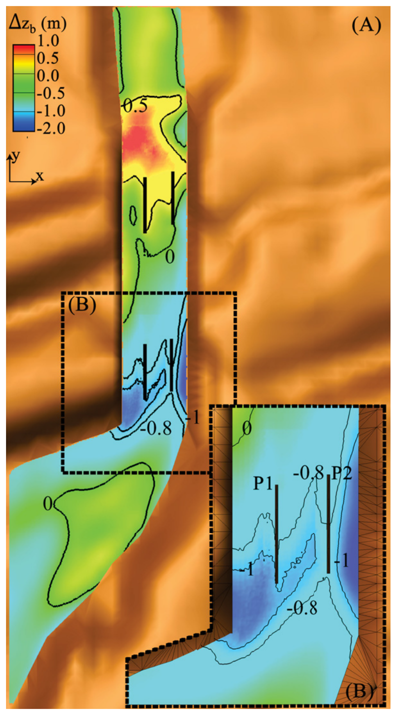

Figure 10: Computed contours of the bed-elevation change (Δz_b) in the Tex wash after $t = 10\ h$ of the flash flood (A). (B) is a zoomed-in window showing details of the computed bed-elevation change around the bridge piers "P1" and "P2". Contour-line labels are in m. Negative and positive values of Δz_b represent scour and deposition. The flash flood flows from bottom to top.

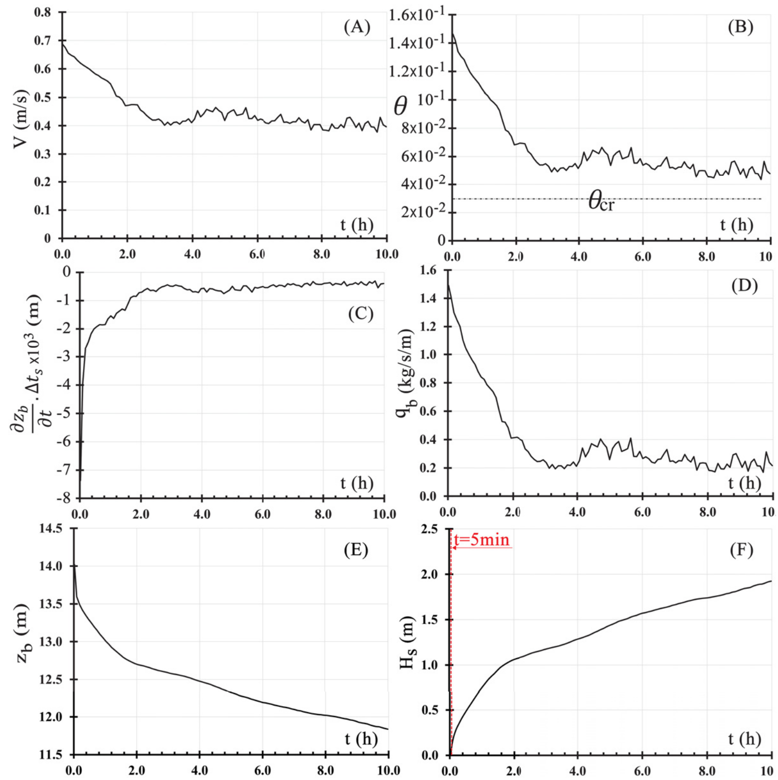

Figure 11: Computed time history of sediment-transport kinematics on the bed surface of the wash at point "th", shown in Fig. 8. (A), (B), (C), (D), (E), and (F) represent the time history of sediment phase velocity magnitude, Shield's parameter, rate of bed-elevation change, sediment bed-load per unit width, bed elevation, and scour depth. In (B), $\theta_c r$ is the threshold value of the θ for sediment movement. Abscissa is time (t) in hours (h).

catchments combining hydrodynamic and hydrological techniques, Journal of Hydrology 540 (2016) 331–339.

[5] L. Boithias, S. Sauvage, A. Lenica, H. Roux, K.C. Abbaspour, K. Larnier, D. Dartus, J.M. Sánchez-Pérez, Simulating flash floods at hourly time-step using the SWAT model, Water 9 (2017) 929.

[6] M. Borga, E.N. Anagnostou, G. Blschl, J.D. Creutin, Flash floods: Observations and analysis of hydro-meteorological controls, Journal of Hydrology 394 (2010) 1–3. Flash Floods: Observations and Analysis of Hydrometeorological Controls.

[7] I. Braud, P.A. Ayral, C. Bouvier, F. Branger, G. Delrieu, J. Le Coz, G. Nord, J.P. Vandervaere, S. Anquetin, M. Adamovic, J. Andrieu, C. Batiot, B. Boudevillain, P. Brunet, J. Carreau, A. Confoland, J.F. Didon-Lescot, J.M. Domergue, J. Douvinet, G. Dramais, R. Freydier, S. Gérard, J. Huza, E. Leblois, O. Le Bourgeois, R. Le Boursicaud, P. Marchand, P. Martin, L. Nottale, N. Patris, B. Renard, J.L. Seidel, J.D. Taupin, O. Vannier, B. Vincendon, A. Wijbrans, Multi-scale hydrometeorological observation and modelling for flash flood understanding, Hydrology and Earth System Sciences 18 (2014) 3733–3761.

[8] J.D. Bricker, W. Schwanghart, B.R. Adhikari, S. Moriguchi, V. Roeber, S. Giri, Performance of Models for Flash Flood Warning and Hazard Assessment: The 2015 Kali Gandaki Landslide Dam Breach in Nepal, Mountain Research and Development 37 (2017) 5–15.

[9] Z. Cao, G. Pender, P. Carling, Shallow water hydrodynamic models for

hyperconcentrated sediment-laden floods over erodible bed, Advances in Water Resources 29 (2006) 546–557.

[10] K. El Kadi Abderrezzak, A. Paquier, E. Mignot, K.E.K. Abderrezzak, A. Paquier, E. Mignot, Modelling flash flood propagation in urban areas using a two-dimensional numerical model, Natural Hazards 50 (2009) 433–460.

[11] J. Gourley, J. M. Erlingis, Y. Hong, E. B. Wells, Evaluation of tools used for monitoring and forecasting flash floods in the united states, Weather and Forecasting 27 (2012) 158–173.

[12] X. Hu, L. Song, Hydrodynamic modeling of flash flood in mountain watersheds based on high-performance gpu computing, Natural Hazards 91 (2018) 567–586.

[13] X. Hu, L. Song, Hydrodynamic modeling of flash flood in mountain watersheds based on high-performance GPU computing, Natural Hazards 91 (2018) 567–586.

[14] P.Y. Julien, M. Velleux, J. John F. England, J. Halgren, J. England, J. Halgren, Flash Flood and Sediment Modeling with TREX, in: Keynote Address in Innovations in Water Resources and Environmental Engineering, Proceedings of the International Conference on Construction and Building Technology, pp. 1–20.

[15] S. Kang, F. Sotiropoulos, Numerical modeling of 3D turbulent free surface flow in natural waterways, Adv. Water Resour. 40 (2012) 23–36.

[16] S. Kara, M.C. Kara, T. Stoesser, T.W. Sturm, Free-surface versus rigid-lid LES computations for bridge-abutment flow, Journal of Hydraulic Engineering 141 (2015) 04015019.

[17] A. Khosronejad, M.G. Aarabi, D. Angelidis, E. Bagherizade, K. Flora, A. Farhadzadeh, Comparative hydrodynamic study of rigid-lid and level-set methods for LES of open-channel flow, Journal of Hydraulic Engineering 145 (2018) 04018077.

[18] A. Khosronejad, M.G. Aarabi, D. Angelidis, E. Bagherizade, K. Flora, A. Farhadzadeh, A comparative study of rigid-lid and level-set methods for LES of open-channel flows: morphodynamics, Environmental Fluid Mechanics (2019).

[19] A. Khosronejad, P. Diplas, D. Angelidis, Z. Zhang, N. Heydari, F. Sotiropouylos, Scour depth prediction at the base of longitudinal walls: a combined experimental, numerical, and field study, Environmental Fluid Mechanics (2019).

[20] A. Khosronejad, A.M. Ghazian, D. Angelidis, E. Bagherzad, K. Flora, A. Farhadzade, Comparative hydrodynamics study of rigid-lid and level-set methods for LES of open-channel flow, Journal of Hydraulic Engineering 145 (2019) 0401807.

[21] A. Khosronejad, S. Kang, I. Borazjani, F. Sotiropoulos, Curvilinear immersed boundary method for simulating coupled flow and bed morphodynamic interactions due to sediment transport phenomena, Advances in Water Resources 34(7) (2011) 829–843.

[22] A. Khosronejad, J. Kozarek, P. Diplas, C. Hill, R. Jha, P. Chatanantavet, N. Heydari, F. Sotiropoulos, Simulation-based optimization of in-stream structures design: rock vanes, Environ. Fluid Mech. 18 (2018) 695–738.

[23] A. Khosronejad, J.L. Kozarek, F. Sotiropoulos, Simulation-based approach for stream restoration structure design: model development and validation, Journal of Hydraulic Engineering 140 (2014) 04014042.

[24] A. Khosronejad, T. Le, P. DeWall, N. Bartelt, S. Woldeamlak, X. Yang, F. Sotiropoulos, High-fidelity numerical modeling of the upper mississippi river under extreme flood condition, Advances in Water Resources 98 (2016) 97 – 113.

[25] A. Khosronejad, F. Sotiropoulos, Numerical simulation of sand waves in a turbulent open channel flow, Journal of Fluid Mechanics 753 (2014) 150–216.

[26] A. Khosronejad, F. Sotiropoulos, On the genesis and evolution of barchan dunes: Morphodynamics, Journal of Fluid Mechanics 815 (2017).

[27] E.W. Knocke, Modeling Flash Floods in Small Ungaged Watersheds using Embedded GIS, Ph.D. thesis, Virginia Tech, 2006.

[28] N.N. Kourgialas, G.P. Karatzas, A hydro-sedimentary modeling system for flash flood propagation and hazard estimation under different agricultural practices, Natural Hazards and Earth System Sciences 14 (2014) 625–634.

[29] N.N. Kourgialas, G.P. Karatzas, N.P. Nikolaidis, Development of a thresholds approach for real-time flash flood prediction in complex geomorphological river basins, Hydrological Processes 26 (2012) 1478–1494.

[30] D. Kvočka, R. Ahmadian, R.A. Falconer, Flood inundation modelling of flash floods in steep river basins and catchments, Water 9 (2017) 705.

[31] B. Li, M. Phillips, C.A. Fleming, Application of 3D hydrodynamic model to flood risk assessment, Proceedings of the Institution of Civil Engineers-Water Management 159 (2006) 63–75.

[32] J. Lian, W. Yang, K. Xu, a. et, Flash flood vulnerability assessment for small catchments with a material flow approach, Natural Hazards 88 (2017) 699–719.

[33] Q. Liu, Y. Qin, Y. Zhang, Z. Li, A coupled 1D–2D hydrodynamic model for flood simulation in flood detention basin, Natural hazards 75 (2015) 1303–1325.

[34] W.C. Liu, W.B. Chen, M.H. Hsu, J.C. Fu, Dynamic routing modeling for flash flood forecast in river system, Natural Hazards 52 (2010) 519–537.

[35] R. Marsooli, P.M. Orton, N. Georgas, A.F. Blumberg, Three-dimensional hydrodynamic modeling of coastal flood mitigation by wetlands, Coastal Engineering 111 (2016) 83–94.

[36] S.M. Mudd, Investigation of the hydrodynamics of flash floods in ephemeral channels: scaling analysis and simulation using a shock-

capturing flow model incorporating the effects of transmission losses, Journal of Hydrology 324 (2006) 65–79.

[37] P. Nguyen, A. Thorstensen, S. Sorooshian, K. Hsu, A. AghaKouchak, B. Sanders, V. Koren, Z. Cui, M. Smith, A high resolution coupled hydrologic–hydraulic model (HiResFlood-UCI) for flash flood modeling, Journal of Hydrology 541 (2016) 401–420.

[38] P. Nguyen, A. Thorstensen, S. Sorooshian, K. Hsu, A. Aghakouchak, B. Sanders, V. Koren, Z. Cui, M. Smith, A high resolution coupled hydrologic-hydraulic model (HiResFlood-UCI) for flash flood modeling, Journal of Hydrology 541 (2016) 401–420.

[39] L.C. van Rijn, Principles of sediment transport in rivers, estuaries, and coastal seas, Aqua Publications, 1993.

[40] M. Roca, M. Davison, Two dimensional model analysis of flash-flood processes: application to the Boscastle event, Journal of Flood Risk Management 3 (2010) 63–71.

[41] M. Schaffner, C. Unkrich, D. Goodrich, A. Tardy, J. Laber, Modeling Flash Flood Events in an Ungaged Semi-Arid Basin using a Real-Time Distributed Model: Fish Creek near Anza Borrego, California, National Oceanic and Atmospheric Administration Western Regional Technical Attachment. (2014) 42 p.

[42] F. Sotiropoulos, A. Khosronejad, Sand waves in environmental flows: Insights gained by coupling large-eddy simulation with morphodynamics, Phys. Fluids 28 (2016) 021301.

[43] M. Tabbakhha, A. Astaneh-Asl, D.C. Setioso, Failure analysis of flood collapse of the tex-wash bridge, in: Proceedings of the World Congress on Civil, Structural, and Environmental Engineering (CSEE16), IC-SENM 118, Prague, Czech Republic.

[44] L.C. Van Rijn, Principles of sediment transport in rivers, estuaries, and coastal seas, Aqua Publications, 1993.

[45] T. Wu, X. Xia, Q. Liang, X. Ming, J. Hou, An efficient and stable hydrodynamic model with novel source term discretization schemes for overland flow and flood simulations, Water Resources Research 53 (2017) 3730–3759.

[46] L. Yang, J.A. Smith, M.L. Baeck, Y. Zhang, Flash flooding in small urban watersheds: Storm event hydrologic response, Water Resources Research 52 (2016) 4571–4589.